RSC Advances

PAPER

View Article Online
View Journal | View Issue

Cite this: *RSC Adv.*, 2016, **6**, 24603

A highly efficient potassium-treated Au–Cu/Al_2O_3 catalyst for the preferential oxidation of carbon monoxide†

Yu-Xin Miao, Lei Shi, Qiang Sun and Wen-Cui Li*

Received 12th October 2015
Accepted 22nd February 2016

DOI: 10.1039/c5ra21119k

www.rsc.org/advances

At the operating temperature (80–120 °C) of a proton exchange membrane fuel cell (PEMFC), high-efficiency elimination of CO while minimizing the H_2 consumption processes is highly desired but still remains a challenge. In the present manuscript, one novel potassium-treated Au–Cu/Al_2O_3 catalyst was synthesized *via* a two step deposition–precipitation (DP) method with excellent catalytic performance for preferential oxidation of CO (CO-PROX) in a H_2-rich stream. This catalyst exhibits 100% CO conversion over a wide temperature window of 60–110 °C and ≥50% selectivity of CO_2 under the PEMFC operating temperature. Furthermore, the as-prepared potassium-treated Au–Cu/Al_2O_3 catalysts were also characterized by N_2 adsorption analysis, scanning transmission electron microscopy (STEM)-energy dispersive X-ray spectroscopy (EDX), and *in situ* diffuse reflectance infrared Fourier transform spectroscopy (*in situ* DRIFTS), and the reasons for enhanced catalytic activity of the potassium-treated sample were elucidated. The introduction of copper could strengthen the CO adsorption on the Au–Cu/Al_2O_3 catalyst and potassium treatment could significantly increase the stability of active Cu^+ species that contribute to enhanced catalytic performance.

1. Introduction

The greenhouse effect and fine particulate matter emission (PM = 2.5) continue to generate intensive interest in seeking sustainable energy sources that can replace traditional fossil fuels. Fuel cells are an environmentally friendly technology for energy transformation with low pollutant emission. Among various types of fuel cells, the proton exchange membrane fuel cell (PEMFC) is a promising candidate due to its higher energy efficiency and lower operating temperature. However, the Pt-based electrode is severely poisoned by the trace levels of CO (about 10 ppm) in a H_2-rich steam. Therefore, selective and efficient elimination of CO while minimizing the H_2 consumption processes is highly desirable.[1,2]

Preferential oxidation of CO (CO-PROX) has been seen as one of the most simple and effective approaches. To our knowledge, supported noble metal catalysts have been widely investigated for CO oxidation due to their high activity under low-temperature ranges.[3] However, at the operating temperature of the PEMFC (80–120 °C), there are fewer monometallic gold catalysts that are able to reach a 100% CO conversion because of the competitive oxidation of H_2 with elevated reaction temperatures.[4–6] In addition, agglomeration and deactivation of gold nanoparticles (Au NPs), further constrain their practical application.[7,8]

The addition of a second noble/transition metal component such as Pt,[9–11] Pd,[12,13] Ni,[14] Ag,[15,16] especially Cu,[17–19] can enhance the catalytic activity and stability of Au NPs and the use of different supports also has an affect on the catalytic activity. Several workers have described the advantages of Au–Cu bimetallic systems on different supports. Among all the reducible oxide support, ceria is hypothesized to play an important role in the activation of oxygen, and can thus contribute to a high activity for CO-PROX over Au–Cu bimetallic catalysts.[17] However, their selectivity is extremely low (below 50%) for a total conversion of CO at the operating temperature. As for the inert supports, Liu *et al.*[20,21] synthesized Au–Cu/SBA-15 catalysts by a two-step method using $NaBH_4$ as reducing agent and studied for CO oxidation. They found that the catalytic activity was enhanced by the introduction of copper, with good synergy between the gold and copper. Mozer *et al.*[22] prepared a Au–Cu/Al_2O_3 catalyst by the DP method and investigated the effect of Cu loading on the CO-PROX activity. They observed that the low amounts of copper were beneficial for the catalytic selectivity, while the CO conversion was not satisfied (below 100%). There are few of Au–Cu catalysts mentioned above that are able to give an acceptable activity and selectivity at the operating temperature.

In our previous works,[23–25] one Au/Al_2O_3 catalysts using home-made γ-Al_2O_3 with controlled morphology have been constructed and were applied for pure CO oxidation in the

State Key Laboratory of Fine Chemicals, Dalian University of Technology, Dalian 116024, P. R. China. E-mail: wencuili@dlut.edu.cn; Fax: +86-411-84986355; Tel: +86-411-84986355

† Electronic supplementary information (ESI) available. See DOI: 10.1039/c5ra21119k

absence of H_2. It has been demonstrated that the as-prepared catalyst was active and stable for CO oxidation even in the co-presence of CO_2 and H_2O at room temperature.[26] In addition, it is noticed that Fan *et al.* reported that the potassium (K^+) could stabilize the active Cu(I) oxidation state in K–Cu–TiO_2 catalyst, which contributed to a high activity in the selective oxidation of benzyl alcohol.[27] Referring these work, hence, we show a newly potassium-treated Au–Cu/Al_2O_3 catalyst that is highly active in the CO-PROX reaction. In contrast to the previous gold catalysts, the novel potassium-treated Au–Cu/Al_2O_3 catalyst showed a remarkably wide temperature window for total CO conversion. Besides, the selectivity for CO-PROX increased significantly with the introduction of the K ion.

2. Experimental

2.1. Catalyst preparation

All the chemicals used in the current work were of analytical grade without further purification. Alumina hollow microsphere support was prepared by a hydrothermal method according to our previous work.[23] The Cu/Al_2O_3 catalyst was prepared by the deposition–precipitation (DP) method. The required amount of $Cu(NO_3)_2 \cdot 9H_2O$ (61 μL, 0.1 M) solution was added into the Al_2O_3/H_2O suspension and the pH value was controlled to *ca.* 8 by addition of $(NH_4)_2CO_3$ (200 μL, 0.5 M) solution dropwise. The mixture was stirred at 60 °C for 2 h. After centrifugation and drying under vacuum, the Cu/Al_2O_3 catalyst was obtained. In the second step, the Au–Cu bimetallic catalyst was also prepared by the DP method. All the steps described below were carried out under exclusion of light by covering the round-bottom flask with aluminum foil. Gold was deposited onto the surface of Cu/Al_2O_3 by using $HAuCl_4$ solution (152 μL, 7.888 g L^{-1}) as the gold precursor and $(NH_4)_2CO_3$ as precipitant, similar to the Cu/Al_2O_3 catalyst preparation procedure described above. For comparison, the Au/Al_2O_3 catalyst was made by the DP method, following the previously reported procedure.[26] The Au loading for each catalyst was 1 wt% and the nominal Au/Cu mole ratio was 1 : 1. This sample is denoted as Au–Cu/Al_2O_3. Potassium-treated Au–Cu/Al_2O_3 catalyst was prepared by an incipient wetness impregnation method. Typically, the required amount of KNO_3 (200 μL) solution was added dropwise to 0.12 g of Au–Cu/Al_2O_3 catalyst under manual stirring for 0.5 h. The mixture was then dried under vacuum overnight. The obtained potassium-treated Au–Cu bimetallic catalyst was denoted as Au–Cu/K–Al_2O_3.

2.2. Activity test

The catalytic performance for CO-PROX was carried out in a fixed-bed flow quartz reactor (8 mm i.d.). The reaction mixture consisted of 1 vol% CO, 1 vol% O_2 and 40 vol% H_2 in N_2 and was allowed to pass through 100 mg of catalyst sample at a total flow rate of 67 mL min^{-1} and the corresponding space velocity was 40 000 mL h^{-1} $g_{cat}{}^{-1}$. When H_2O and CO_2 were added to the reaction flow, the gas contained 1 vol% CO + 1 vol% O_2 + 40 vol% H_2 + (20 vol% CO_2 or 10 vol% H_2O) balanced with N_2, while the space velocity was 80 000 mL h^{-1} $g_{cat}{}^{-1}$. Prior to the catalytic evaluation, the catalyst was *in situ* reduced with H_2 at 250 °C for 2 h. The effluent gas was analyzed on-line by a gas chromatograph (Tianmei GC-7890) with packed 5A molecular sieve column and equipped with a thermal conductivity detector (TCD). The CO conversion and CO_2 selectivity were calculated as follows:

$$\text{CO conversion (\%)} = (CO_{in} - CO_{out})/CO_{in} \times 100$$

$$CO_2 \text{ selectivity (\%)} = (CO_{in} - CO_{out})/2(O_{2\ in} - O_{2\ out}) \times 100$$

2.3. Catalyst characterization

The actual loadings of Au, Cu and K were determined by inductively coupled plasma atomic emission spectrometer (ICP-AES) on the Optima 2000 DV. Nitrogen adsorption isotherms were measured using a Micromeritics Tristar 3000 instrument. All the samples were heated to 200 °C under vacuum for 4 h to remove all adsorbed species. The Brunauer–Emmett–Teller (BET) method was utilized to calculate the specific surface areas (S_{BET}). The morphologies of Au–Cu/K–Al_2O_3 catalyst was characterized with a FEI Quanta 450 instrument microscope equipped with a cooled energy-dispersive X-ray (EDX) spectrometer from Oxford Instruments for point resolved elemental analysis. Transmission electron microscope (TEM) images were obtained with a FEI Tecnai G220 S-Twin microscope with an accelerative voltage of 200 kV. Scanning transmission electron microscopy (STEM) and energy-dispersive X-ray (EDX) were performed with FEI Tecnai F30 electron microscope at an accelerating voltage of 300 kV. *In situ* diffuse reflectance FTIR spectra (DRIFTS) were recorded by a Nicolet 6700 FT-IR spectrometer equipped with MCT detector and diffuse reflectance cell. The catalyst was heated to 200 °C for 30 min under vacuum prior to the test. The background spectrum was collected in a flowing He atmosphere at the desired temperature and *in situ* DRIFTS data were collected in 5 vol% CO/He atmosphere at 20 min. Infrared Fourier transform spectra (FT-IR) were also recorded using a Nicolet 6700 FT-IR spectrometer at a resolution of 4 cm^{-1} and scale at 4000–640 cm^{-1}.

3. Results and discussion

3.1. Catalytic activity and stability in the CO-PROX

Fig. 1a and b shows the catalytic activity and selectivity for CO-PROX of different catalysts. For Au/Al_2O_3 catalyst, the maximum conversion of CO was 100% and the selectivity of CO_2 was 59% at 60 °C. However, the CO conversion was decreased dramatically by H_2 oxidation taking place when raising the reaction temperature. For comparison, one monometallic Cu/Al_2O_3 catalyst was also tested. The Cu/Al_2O_3 catalyst was completely inactive for CO-PROX over the temperature range of 30–150 °C due to the low Cu contents (0.3 wt%). It can be clearly seen that the Au–Cu/Al_2O_3 sample shows the best results which gave a 100% CO conversion over a wide temperature window of 50–100 °C and 50% selectivity of CO_2 in the operating temperature of PEMFC. The 100% selectivity is observed only between 30 and 50 °C. The improved catalytic performance of the Au catalysts

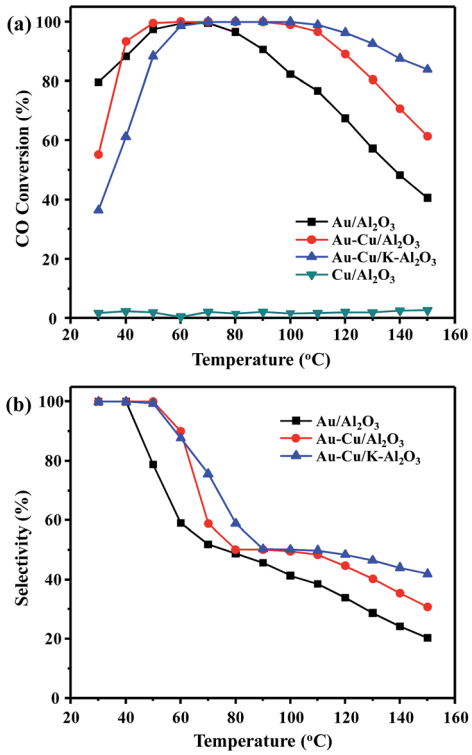

Fig. 1 (a) Conversion and (b) selectivity as a function of the reaction temperature for CO-PROX over Au–Cu/Al_2O_3 catalysts. Reaction conditions: 1 vol% CO + 1 vol% O_2 + 40 vol% H_2 and balance N_2. Weight hourly space velocity (WHSV) = 40 000 mL h^{-1} g_{cat}^{-1}.

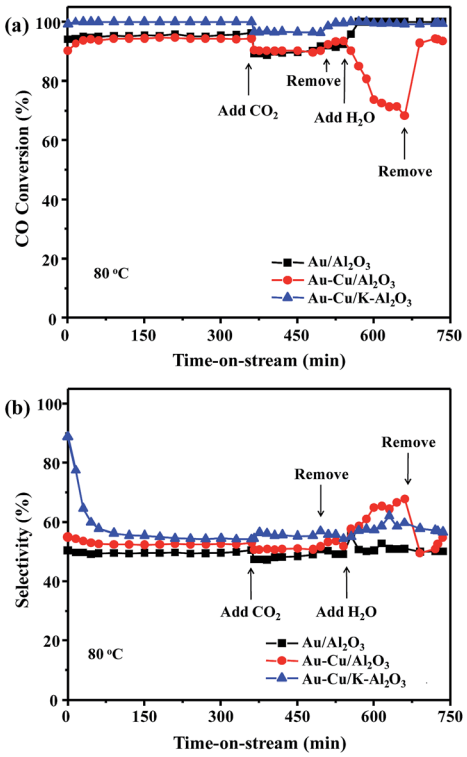

Fig. 2 Stability test over Au/Al_2O_3, Au–Cu/Al_2O_3 and Au–Cu/K–Al_2O_3 catalysts with the time-on-stream at 80 °C. (a) Conversion and (b) selectivity for CO-PROX. Reaction conditions: 1 vol% CO + 1 vol% O_2 + 40 vol% H_2 + (20 vol% CO_2 or 10 vol% H_2O) and balance N_2. WHSV = 80 000 mL h^{-1} g_{cat}^{-1}.

can be ascribed to the synergistic effect between gold and copper. The presence of Cu enhanced the catalytic performance of the Au/Al_2O_3 catalyst. Moreover, the addition of a higher copper content seemed to block gold active sites and lead to lower activity for the CO-PROX reaction.[17,18,22]

In order to improve the selectivity of these Au–Cu catalysts, the potassium nitrate with different content was selected as an additive. These results are depicted in Fig. S1a and S1b.† It can be seen that the Au–Cu/K–Al_2O_3 catalyst with 2% K^+ content exhibited a 100% CO conversion over a wide temperature window of 60–110 °C and 60% selectivity of CO_2 under the PEMFC operating temperature. As expected, the temperature window of CO total conversion increased for the Au–Cu/K–Al_2O_3 catalyst, which was more selective in comparison with Au–Cu/Al_2O_3 (50% selectivity). However, the CO conversion decreased drastically by further addition of K^+ (3–7%), revealing the negative effect of this promoter. The effect of optimum temperature window was greatly dependent on the amount of additive, and the 2 wt% of potassium was appropriate. These results indicated that the addition of potassium to Au–Cu catalyst promotes the CO_2 selectivity in CO-PROX. Furthermore, compared with other gold catalysts reported in CO-PROX reaction recently, the as-prepared Au–Cu/K–Al_2O_3 catalyst was actually the most impressive one.[17,19,20,22]

The stability test of Au/Al_2O_3, Au–Cu/Al_2O_3 and Au–Cu/K–Al_2O_3 catalysts at operating temperature (80 °C) was conducted. From Fig. 2a and b, it is clearly seen that the Au–Cu catalysts were stable over a 6 h run in the absence of H_2O or CO_2. In the presence of CO_2 or H_2O, the Au–Cu/K–Al_2O_3 sample gave a higher CO conversion (*ca.* 100%) and selectivity of CO_2 (*ca.* 60%) compared with Au/Al_2O_3 and Au–Cu/Al_2O_3 catalysts. The Cu-based catalysts, including in combination with Au–Cu NPs, exhibited poor resistance toward CO_2 and H_2O, which is often observed for Cu-based catalysts such as Hopcalite catalyst. After adding 10 vol% H_2O into the feed gases, the Au–Cu/Al_2O_3 sample lost activity very quickly (from 94% to 70%) at a high space velocity (80 000 mL h^{-1} g_{cat}^{-1}), which is due to the CO_2 adsorption on the Cu surface in the presence of H_2O. However, the catalytic performance can be recovered when removing the H_2O.

3.2. Textural and morphological properties

To obtain the structure and texture information of Au–Cu catalysts, a number of characterization studies including N_2 adsorption, SEM, EDX, TEM and HAADF-STEM were performed. The corresponding specific surface areas and total pore volumes of representative samples are listed in Table 1. The specific surface areas and the total pore volumes of Au–Cu/Al_2O_3, and Au–Cu/K–Al_2O_3 were similar. These results demonstrated that the specific surface area and pore structure of Au–Cu catalysts were slightly affected by potassium doped. The ICP-AES result shows that the weight percentage of gold, copper and potassium

Table 1 Physicochemical properties of different supported Au–Cu catalysts

Catalyst	Au : Cu (mol)	Au theoretical loading (wt%)	Au actual loading[a] (wt%)	Cu loading[a] (wt%)	K loading[a] (wt%)	S_{BET} ($m^2\ g^{-1}$)	V_{total} ($cm^3\ g^{-1}$)	Rate[b] (mol h^{-1} g_{Au}^{-1})
Al_2O_3	—	—	—	—	—	158	0.60	—
Au/Al_2O_3	—	1.0	0.92	—	—	160	0.56	1.561
$Au–Cu/Al_2O_3$	1 : 1	1.0	0.97	0.38	—	161	0.63	1.018
$Au–Cu/K–Al_2O_3$	1 : 1	1.0	0.98	0.34	1.95	144	0.62	0.659

[a] The actual loadings of Au, Cu and K were determined by an ICP technique. [b] The reaction rate is evaluated at 30 °C.

of $Au–Cu/K–Al_2O_3$ was *ca.* 0.98 wt%, 0.34 wt% and 1.95 wt%, respectively, and so very close to the theoretical values.

The TEM images of $Au–Cu/Al_2O_3$ and $Au–Cu/K–Al_2O_3$ catalysts are shown in Fig. 3a and b, which indicate a very small and uniform particle size distribution. Therefore, we further studied the $Au–Cu/K–Al_2O_3$ catalyst using an HAADF-STEM technique and used the average Au–Cu particle size for evaluation.[28,29] From Fig. 3c and d, it was found that all the Au–Cu NPs are highly dispersed. One can see that the average metal particle size of the $Au–Cu/K–Al_2O_3$ was approximately 2 nm on the Al_2O_3 surface, which presence was confirmed by EDX (Fig. 3e and f).

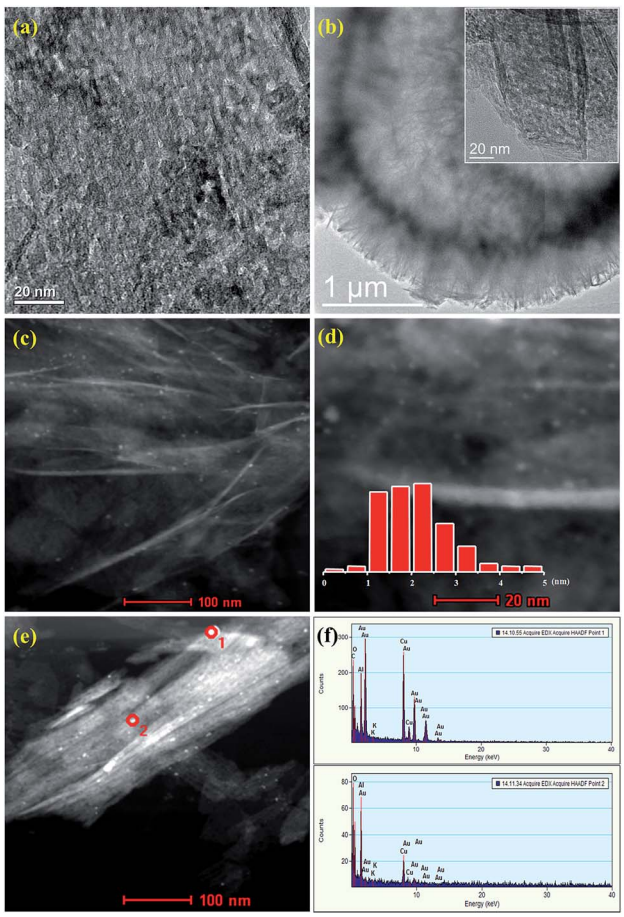

Fig. 3 TEM images of $Au–Cu/Al_2O_3$ (a) and $Au–Cu/K–Al_2O_3$ (b), HAADF-STEM images of $Au–Cu/K–Al_2O_3$ (c–e), (f) the corresponding EDX patterns based on the selected area shown in (e).

The sizes of Au–Cu agglomerates were less than 5 nm, which is smaller than previously described.[17,18,28,29] Furthermore, the SEM image shows that the hollow structure and morphology of Al_2O_3 microsphere has not changed (Fig. 4a). These hollow microsphere structures are composed of interpenetrating nanoflakes with a diameter of 5–6 μm, which is similar to our recent work.[23,26] Based on the EDX map results, gold, copper and potassium are all uniformly distributed throughout the Al_2O_3 hollow microsphere surface (Fig. 4b–d). The corresponding results further indicate that the Au/Cu molar ratio was nearly 1 : 1, which is in agreement with the ICP-AES analysis. Thus, based on the above results, one can conclude that the highly dispersed Au–Cu catalyst have been little affected by potassium doped.

3.3. FT-IR spectroscopic analysis

To further understand the effect of potassium-treated for the exceptionally high catalytic activity and selectivity of Au–Cu catalyst, *in situ* DRIFT spectra of CO adsorption were carried out. In our previous work of Au/Al_2O_3 catalyst,[26] CO can form carbonyls with different species of gold, such as $Au^{\delta+}$–CO

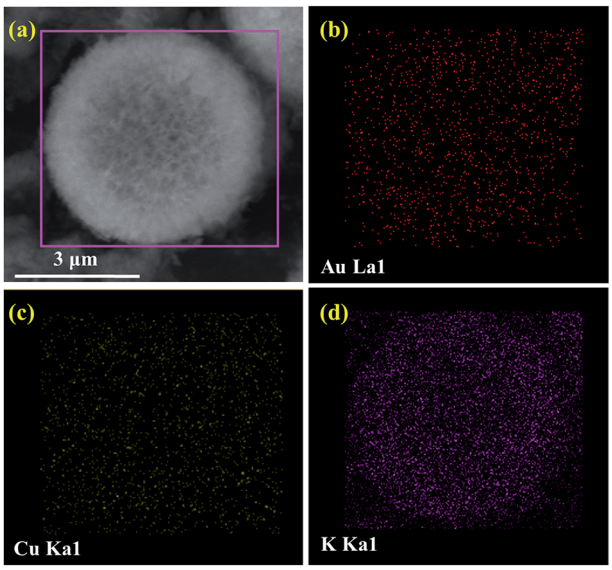

Fig. 4 (a) SEM images of the $Au–Cu/K–Al_2O_3$. Typical EDX (b) gold, (c) copper and (d) potassium maps based on the selected area shown in (a), of the $Au–Cu/K–Al_2O_3$.

(*ca.* 2171 cm^{-1}), Au^0–CO (*ca.* 2114 cm^{-1}) and $Au^{\delta-}$–CO (*ca.* 2056 cm^{-1}). The Au^0–CO and $Au^{\delta-}$–CO bands are observed at low-temperatures only and are easily removed by elevating the adsorption temperatures. It was found that the metallic gold usually provides active sites for CO oxidation. The DRIFT spectra of CO adsorption on Cu/Al_2O_3 are exhibited in Fig. 5a. As the adsorption time is increased, the bands at 2170, 2098 and 2050 cm^{-1} were observed, which can be ascribed to the linear adsorption of Cu^{2+}–CO, Cu^+–CO and Cu^0–CO, respectively.[30,31] On the other hand, the bands at 1951 and 1850 cm^{-1} were assigned to bridged- and multi-bonded CO species on Cu^0.[32] These bands remained almost constant, whereas the band of Cu^+–CO around at 2098 cm^{-1} increased.

As shown in Fig. 5b, when the $Au–Cu/Al_2O_3$ catalyst was exposed to CO for 20 min at 30 °C, several similar characteristic peaks around at *ca.* 2171 and 2056 cm^{-1} were also observed on the $Au–Cu/Al_2O_3$ catalyst. One smaller band appeared at *ca.* 2105 cm^{-1}, which could be ascribed to the strong geometric effect between Au and Cu (Au^0/Cu^+–CO).[33] Similar adsorption behavior was also reported on the $Au–Cu/TiO_2$ catalyst.[32] Moreover, the intensity of the main carbonyl band ($Au^{\delta-}$–CO) increases with time and the $Au–Cu/Al_2O_3$ catalyst reached equilibrium of CO adsorption after 10 min, indicate that the CO adsorption rate is higher than the Cu/Al_2O_3 sample (Fig. 5a). During heating up the CO-adsorption temperatures from 30 to 150 °C (Fig. 5c), the intensities of the peaks gradually decreased and disappeared as for the band of $Au^{\delta-}$–CO (*ca.* 2056 cm^{-1}). This is due to the decreasing CO coverage of the Au nanoparticles. Simultaneously, a new band was appeared at 2340 cm^{-1} which could be ascribed to the CO_2, suggesting that CO can be oxidized.[26] It should be noted that the weak absorption band of Cu^+–CO (*ca.* 2098 cm^{-1}) remained unchanged, which

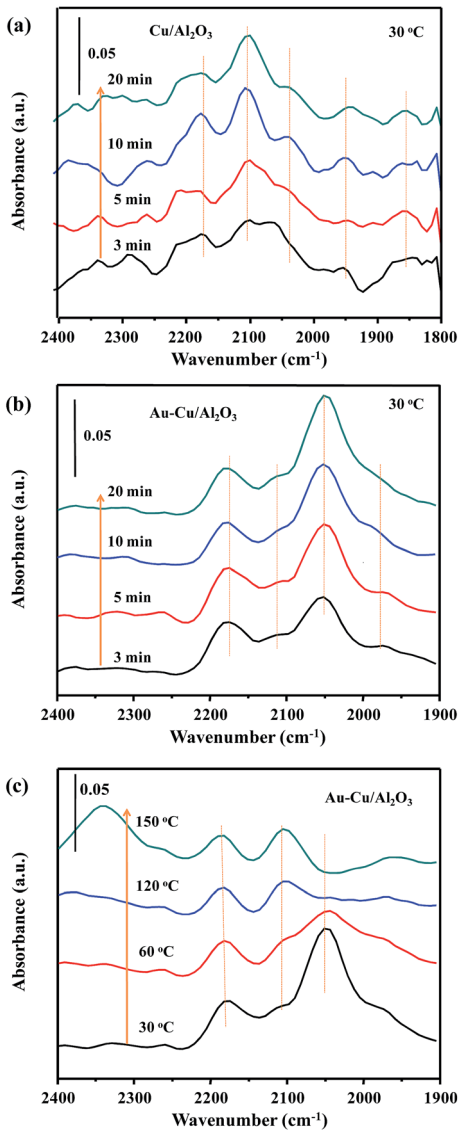

Fig. 5 DRIFT spectra of CO adsorption on (a) Cu/Al_2O_3, (b) $Au–Cu/Al_2O_3$ at 30 °C, (c) $Au–Cu/Al_2O_3$ with different adsorption temperature.

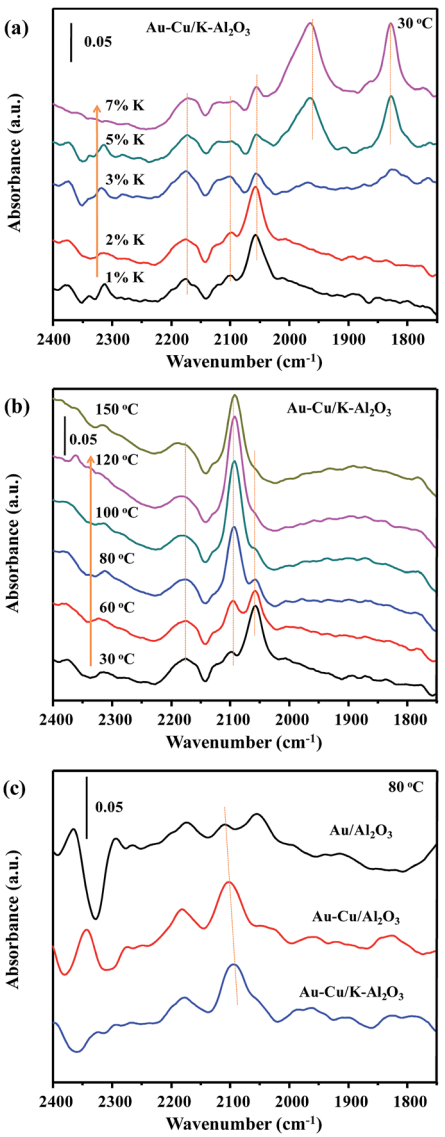

Fig. 6 DRIFT spectra of CO adsorption on (a) $Au–Cu/K–Al_2O_3$ catalysts with different K loadings and (b) $Au–Cu/K–Al_2O_3$ with different adsorption temperature, (c) DRIFT spectra of CO adsorption on different catalysts at 80 °C.

strongly suggests that the Cu^+ species can be promoted in activating CO. The CO adsorption capacity was greatly enhanced and thus contributes a high CO conversion at the operating temperature of PEMFC (80 °C).

Furthermore, the DRIFT spectra of CO adsorption curves obtained at 30 °C over Au–Cu/K–Al_2O_3 catalysts with different potassium doped content are shown in Fig. 6a. The linear adsorption of CO at 2105 and 2050 cm^{-1} decreased with increasing the potassium doped content. Meanwhile, the bridged- and multi-bonded forms of CO species on Cu^0 at 1951 and 1850 cm^{-1} were increased. Therefore, 2% of K doping amount was more appropriate for strong linear adsorption of Cu^+–CO and $Au^{\delta-}$–CO. By raising the CO adsorption temperature from 30 to 150 °C, the intensity of the Au^0/Cu^+–CO band was increased (Fig. 6b). However, the intensity of the adsorption bands assigned to $Au^{\delta-}$–CO and Cu^0–CO were decreased. The data indicate that the CO adsorption on Cu^+ was effectively improved by doping with K (Fig. 6b and 5c). As far as we know, the copper species is one key factor that determines their catalytic performance in CO oxidation due to the active oxygen. Overall, the addition of potassium to Au–Cu catalyst dramatically promotes catalytic selectivity between 80–120 °C. The above results are in agreement with the catalytic selectivity (Fig. 1b).

To investigate the difference between catalytic behaviors of Au–Cu catalyst, DRIFT spectra of CO adsorption study for different catalysts at 80 °C were also performed (Fig. 6c). As for Au–Cu/K–Al_2O_3 samples, the intensity of the bands at 2105 cm^{-1} (Au^0/Cu^+–CO) was stronger than that on the Au/Al_2O_3 and Au–Cu/Al_2O_3 samples at 80 °C. The Au^0/Cu^+–CO peak at 2105 cm^{-1} gradually increased in intensity and shifts to 2094 cm^{-1} with addition of potassium. The red-shift of carbonyl peak is probably caused by the charge-transfer from Cu to Au, which resulted from an obvious enhancement in valence electron density which then gave a stronger electronic back-donation to the π* orbital of CO.[34,35] However, it was also found that the Au–Cu/Al_2O_3 catalyst was easily influenced by the deposition of carbonate species (Fig. 7), resulting in the carbonate-species covering more active sites on its surface, and then causes a negative effect during the CO-PROX reaction (Fig. 2). A similar deactivation process was also reported over the Au/Fe_2O_3 [36] and Au/La-CeO_x[37] catalyst.

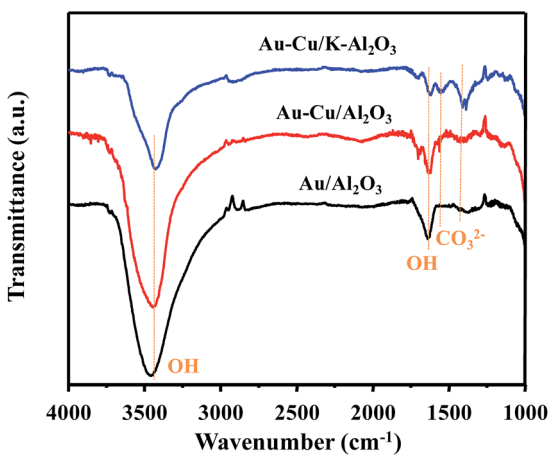

Fig. 7 FT-IR results of carbonate-like species on used catalysts.

4. Conclusions

In summary, a novel potassium-treated Au–Cu catalyst has been successfully synthesized. The catalytic activity (100%) and selectivity (60%) of these catalysts was not only higher than that of reported catalysts for the CO-PROX reaction, but also displayed a wide temperature range (60–110 °C) for 100% CO conversion for CO oxidation under PEMFC operation conditions. *In situ* DRIFTS have demonstrated that the introduction of copper could strengthen the CO adsorption on these Au–Cu catalysts. Meanwhile the stability of active Cu^+ species could be significantly enhanced by potassium-treated which increases the catalytic selectivity for the CO-PROX reaction. Overall, this potassium-treated Au–Cu NPs provides an innovative approach to design gold based catalysts for potential application in the future.

Acknowledgements

Financial supports from the National Program on Key Basic Research Project (No. 2013CB934104) and National Natural Science Foundation of China (No. U1462120) are greatly acknowledged.

Notes and references

1 S. Ahmed and M. Krumpelt, *Int. J. Hydrogen Energy*, 2001, **26**, 291–301.
2 C.-J. Winter, *Int. J. Hydrogen Energy*, 2011, **36**, 12653–12654.
3 H. Zhu, Z. Wu, D. Su, G. M. Veith, H. Lu, P. Zhang, S.-H. Chai and S. Dai, *J. Am. Chem. Soc.*, 2015, **137**, 10156–10159.
4 P. Landon, J. Ferguson, B. E. Solsona, T. Garcia, A. F. Carley, A. A. Herzing, C. J. Kiely, S. E. Golunski and G. J. Hutchings, *Chem. Commun.*, 2005, 3385–3387.
5 W.-Y. Yu, C.-P. Yang, J.-N. Lin, C.-N. Kuo and B.-Z. Wan, *Chem. Commun.*, 2005, 354–356.
6 Q. Lin, B. Qiao, Y. Huang, L. Li, J. Lin, X. Y. Liu, A. Wang, W.-C. Li and T. Zhang, *Chem. Commun.*, 2014, **50**, 2721–2724.
7 C. T. Campbell, S. C. Parker and D. E. Starr, *Science*, 2002, **298**, 811–814.
8 N. Bion, F. Epron, M. Moreno, F. Mariño and D. Duprez, *Top. Catal.*, 2008, **51**, 76–88.
9 A. U. Nilekar, S. Alayoglu, B. Eichhorn and M. Mavrikakis, *J. Am. Chem. Soc.*, 2010, **132**, 7418–7428.
10 T. A. Yamamoto, T. Nakagawa, S. Seino and H. Nitani, *Appl. Catal., A*, 2010, **387**, 195–202.
11 K. Liu, A. Wang and T. Zhang, *ACS Catal.*, 2012, **2**, 1165–1178.
12 J. Xu, T. White, P. Li, C. He, J. Yu, W. Yuan and Y.-F. Han, *J. Am. Chem. Soc.*, 2010, **132**, 10398–10406.
13 K. Qian and W. Huang, *Catal. Today*, 2011, **164**, 320–324.
14 X. Xu, Q. Fu, X. Guo and X. Bao, *ACS Catal.*, 2013, **3**, 1810–1818.

15 T. Déronzier, F. Morfin, M. Lomello and J.-L. Rousset, *J. Catal.*, 2014, **311**, 221–229.
16 A. Sandoval, A. Aguilar, C. Louis, A. Traverse and R. Zanella, *J. Catal.*, 2011, **281**, 40–49.
17 X. Liao, W. Chu, X. Dai and V. Pitchon, *Appl. Catal., B*, 2013, **142–143**, 25–37.
18 X. Liu, A. Wang, T. Zhang, D.-S. Su and C.-Y. Mou, *Catal. Today*, 2011, **160**, 103–108.
19 X. Li, S. S. S. Fang, J. Teo, Y. L. Foo, A. Borgna, M. Lin and Z. Zhong, *ACS Catal.*, 2012, **2**, 360–369.
20 X. Liu, A. Wang, X. Wang, C. Mou and T. Zhang, *Chem. Commun.*, 2008, 3187–3189.
21 X. Liu, A. Wang, L. Li, T. Zhang, C.-Y. Mou and J.-F. Lee, *J. Catal.*, 2011, **278**, 288–296.
22 T. S. Mozer, D. A. Dziuba, C. T. P. Vieira and F. B. Passos, *J. Power Sources*, 2009, **187**, 209–215.
23 J. Wang, Z.-H. Hu, Y.-X. Miao and W.-C. Li, *Gold Bull.*, 2014, **47**, 95–101.
24 J. Wang, K. Shang, Y. Guo and W.-C. Li, *Microporous Mesoporous Mater.*, 2013, **181**, 141–145.
25 J. Wang, A.-H. Lu, M. Li, W. Zhang, Y.-S. Chen, D.-X. Tian and W.-C. Li, *ACS Nano*, 2013, **7**, 4902–4910.
26 Y.-X. Miao, L. Shi, Li.-Na. Cai and W.-C. Li, *Gold Bull.*, 2014, **47**, 275–282.
27 J. Fan, Y. Dai, Y. Li, N. Zheng, J. Guo, X. Yan and G. D. Stucky, *J. Am. Chem. Soc.*, 2009, **131**, 15568–15569.
28 C. Pojanavaraphan, A. Luengnaruemitchai and E. Gulari, *Appl. Catal., A*, 2013, **456**, 135–143.
29 C. Pojanavaraphan, A. Luengnaruemitchai and E. Gulari, *Int. J. Hydrogen Energy*, 2013, **38**, 1348–1362.
30 L. Cai, Z. Hu, P. Branton and W. Li, *Chin. J. Catal.*, 2014, **35**, 159–167.
31 D. Gamarra and A. Martínez-Arias, *J. Catal.*, 2009, **263**, 189–195.
32 A. Sandoval, C. Louis and R. Zanella, *Appl. Catal., B*, 2013, **140–141**, 363–377.
33 V. Ponec, *Adv. Catal.*, 1983, **32**, 149–214.
34 M. Kuhn and T. K. Sham, *Phys. Rev. B: Condens. Matter Mater. Phys.*, 1994, **49**, 1647–1661.
35 L. Ouyang, G.-J. Da, P.-F. Tian, T.-Y. Chen, G.-D. Liang, J. Xu and Y.-F. Han, *J. Catal.*, 2014, **311**, 129–136.
36 M. M. Schubert, A. Venugopal, M. J. Kahlich, V. Plzak and R. J. Behm, *J. Catal.*, 2004, **222**, 32–40.
37 A. Luengnaruemitchai, S. Chawla and R. Wanchanthuek, *Int. J. Hydrogen Energy*, 2014, **39**, 16953–16963.